SOME ASPECTS OF THE RADIO-MAGNETOTELLURIC METHOD AND INSTRUMENTATION DEVELOPMENT

LÁSZLÓ VINCZE

University of Miskolc, Department of Geophysics, laszlo.vincze@student.uni-miskolc.hu https://orcid.org/0000-0002-9272-0560

Abstract: In recent decades, the demand for shallow geophysical methods and instruments has changed significantly. Today, there is a need for methods and instruments that can provide a large amount of accurate measurement results in a short time, which are suitable for developing effective inversion procedures. Only contactless methods can meet the speed requirement. The measurement technique is significantly simplified if we can use a signal source that is of natural origin or an artificial source created for other purposes (e.g. radio transmitters). The radio-magnetotelluric method (RMT), which can be considered an extended variation of the popular very low frequency (VLF) method in terms of frequency range, is exactly such a method. Another advantage is that the created field can be considered a plane wave, thus simplifying the data processing and interpretation procedures. This study presents a brief history of the development of VLF-RMT methods, the evolution of instruments, the development of processing methods, the characteristics of modern inversion methods, and then summarizes the aspects of designing a modern RMT instrument.

Keywords: VLF, RMT, software defined radio, SDR, digital signal processing, DSP

1. Introduction

In the early 1960s, electromagnetic methods were already in full use in exploration geophysics. The theory of magnetotellurics - where the electromagnetic field serving as the basis of the method can be considered as a plane wave - was summarized by Cagniar(1953). In Canada, the Scandinavian countries, mainly Sweden and Finland, and the Soviet Union, induction electromagnetic (Slingram) methods were used to investigate well-conducting massive sulphide ore bodies. The behavior of radio waves and their geological utilization have been studied for a long time by several researchers: Wait (1953), Dosso (1962), Dosso (1965a, 1965b). The theoretical foundations are summarized by McNeil and Labson (1991).

The antennas of VLF and LF radio transmitters can be considered as short vertical electric monopoles on a horizontal conductive plate. Electromagnetic waves propagate directly, as surface waves at the earth-air interface and by reflection from the ionosphere. Since the reception location is usually a long distance, multiples of the wavelength, from the transmitting antenna, the electromagnetic field there can be considered as a plane wave, similar to

magnetotelluric phenomena, therefore the procedures developed there can be applied to the VLF and RMT methods as well. Almost regardless of the angle of incidence at the air-earth interface, due to the high refractive index, the plane wave travels downwards perpendicular to the surface in the subsurface layers. Moving downwards, depending on the resistivity of the medium, the electromagnetic field strengths decrease exponentially. The penetration depth, or skin depth, is the depth at which the amplitude measured at the surface decreases by 1/e (approx. 37%)

$$\delta = \sqrt{\frac{2}{\mu\sigma\omega}} = 503\sqrt{\frac{\rho}{f}} \tag{1}$$

where δ is skin depth, μ is magnetic permeability, σ is conductivity, ρ is resistivity, ω is angular frequency, f is frequency.

Table 1
Skin depth at different frequencies and resistivities

f\ρ	10 Ohmm	30 Ohmm	100 Ohmm	300 Ohmm	1000 Ohmm
15 kHz	13 m	22.5 m	41.1 m	71.2 m	129.9 m
30 kHz	9.2 m	16 m	29.1 m	50.4 m	91.9 m
75 kHz	5.9 m	10.1 m	18.4 m	31.9 m	58.1 m
155 kHz	4.1 m	7 m	12.8 m	22.2 m	40.5 m
240 kHz	3.3 m	5.7 m	10.3 m	17.8 m	32.5 m

It can be seen from Table 1 that the narrow VLF band (bold), depending on the resistivity, allows a depth penetration of a few tens of meters. In the case of bedrock with high resistivity, the penetration depth can reach 100 m depth-selective evaluation of the measurements, even if we measure at all possible frequencies, is only possible to a limited extent. By supplementing the VLF measurements with LF range transmitters (RMT), more possibilities are available for the layer separation with inversion.

At a measurement point far from the VLF-LF transmitters, the electromagnetic field over a homogeneous half-space has horizontal and vertical electric components in the direction of transmission, and horizontal magnetic components perpendicular to the direction of transmission. The ratios of the components (E_x, E_z, H_y) are related to the conductivity (σ_1) of the half-space

$$W = \frac{E_x}{E_z} = \frac{1+i}{\sqrt{2}} \sqrt{\frac{\omega \varepsilon_0}{\sigma_1}}$$
 (2)

$$Z = \frac{E_x}{H_y} = \frac{1+i}{\sqrt{2}} \sqrt{\frac{\omega \mu_0}{\sigma_1}} \tag{3}$$

where W is wave slope; Z - input impedance; ε_0 - dielectric constant of a vacuum; μ_0 is magnetic permeability of the vacuum. The 1+i factor in the equations indicates that there is a 45° phase difference between the components. Since all three field components in the equations can be easily measured, it is possible to determine the conductivity or resistivity of the half-space

$$\rho_a = \frac{1}{\mu \omega} \left| \frac{E_x}{H_y} \right|^2 \tag{4}$$

$$\rho_a = \frac{1}{\varepsilon \omega} \left| \frac{E_X}{E_Z} \right|^2 \tag{5}$$

In the case of 2D and 3D effects, a vertical magnetic component is induced. The VLF-EM method uses only the magnetic components. Since the vertical magnetic component (H_z) is in phase shift (ϕ) with the tangential magnetic component (H_x) , the magnetic field is described by a polarization ellipse (a, b, θ) . Paterson and Ronka (1970) reported on the first experiences of the application of VLF-EM. Saydam (1981) wrote about the interpretation of inclination angle and ellipticity measurements

tilt angle:
$$\tan(2\theta) = \frac{2^{H_Z}/H_X\cos\phi}{1-(H_Z/H_X)^2}$$
 (6)
ellipticity: $\varepsilon = \frac{b}{a} = \frac{H_ZH_X\sin\phi}{|H_Ze^{i\phi}\sin\theta + H_X\cos\theta|^2}$ (7)

ellipticity:
$$\varepsilon = \frac{b}{a} = \frac{H_z H_x \sin \phi}{\left|H_z e^{i\phi} \sin \theta + H_x \cos \theta\right|^2}$$
 (7)

It is worth writing the relationships for the normalized real and quadrature H_z component as well. For small secondary magnetic components, the tilt angle is equal to the real component of the secondary magnetic field, while the ellipticity is equal to the imaginary component

$$H_z(I) = \frac{H_z}{H_x} \cos \phi \; ; H_z(Q) = \frac{H_z}{H_x} \sin \phi \tag{8}$$

$$\tan 2\theta = 2H_z(I) \frac{1}{1 - (H_z/H_x)^2} \cong 2H_z(I)$$
 (9)

$$\varepsilon = H_z(Q) \frac{1}{(H_z(I)\sin\theta + \cos\theta)^2 + (H_z(Q)\sin\theta)^2} \cong H_z(Q)$$
 (10)

In the two-dimensional case, the relationship between the target orientation and the direction of the field components is of great importance. When the electric field is aligned with the structural strike of the target, the configuration is referred to as E-polarization. Conversely, when the magnetic field is parallel to the structural strike, it is referred to as H-polarization. If we measure with only one transmitter, with a VLF wave coming from a given direction, then we speak of scalar measurement. If we measure with VLF waves coming from several directions, then in addition to the slightly different frequency, the measured value will also differ due to the structure being different from 1D. In this case, we speak of tensor measurement. Farkas (1978) proposed a VLF invariant resistance method to eliminate the 2D effect. Pedersen (1998) mentioned the tipper vector for tensor VLF measurements (using at least two or more transmitters). At a given frequency, the vertical component of the magnetic field is linearly related to the horizontal components, where A and B are the components of the tipper vector

$$H_z = AH_x + BH_y \tag{11}$$

2. Interpretation Methods

In the early days of the VLF method, when only magnetic components were measured, the interpretation of the measurements was based on anomalies in the graphical representation of the measurements along the section. The first quantitative data processing was proposed by Fraser (1969). The original goal of the procedure was to filter the data. Four consecutive data are used for filtering. The average of the first two is subtracted from the average of the last two, but the divisions by two are omitted

$$f_{2,3} = (M_3 + M_4) - (M_1 + M_2) \tag{12}$$

where M_i denotes four measurement data (i=1,2,3,4), $f_{2,3}$, is the result of the Fraser filtering applied between points 2 and 3. This gives us the directional derivative of the average data. Filtering reduces noise, suppresses topographic effects, and simplifies the interpretation of anomalies by transforming an asymmetric (sign-changing) dip angle anomaly into an anomaly with a maximum peak.

Kaikkonen (1979) performed 2D numerical modeling for the anisotropic case using the finite element method. He investigated the effect of a tilted, finite plate covered with a layer. He found that in the case of a bad conductor, the inclination angle and the ellipticity polarity are the same, but in the case of a good conductor, the polarity and shape of the ellipticity also change. The inclination of the plate spoils the symmetry of the anomaly. Saydam (1981) reported relationships between the amplitude, width and simple acting parameters (depth, width, etc.) of inclination angle and ellipticity anomalies. Bezvoda and Segeth (1982) investigated the effect and detectability of two adjacent dykes, also using the finite element method. Teemull and Crossley (1982) described an inversion procedure for simple

2D structures where continuous, weak lateral changes can be described using harmonic functions. Karaous and Hjelt (1983) developed a linear filtering procedure for VLF inclination measurements. The result of the filtering is equivalent current densities for different depths. The filtering procedure can be considered an extension of the Fraser filter

$$H_{KH} = -0.201H_{-2} + 0.323H_{-1} - 1.446H_0 + 1.446H_1 - 0.323H_2 + 0.205H_3$$
 (13)

Olsson (1983) investigated a model of a plate in a horizontally layered half-space. McNeil (1991) has a RELACON filter like the Fraser filter but designed to convert VLF magnetic data into relative conductivity data. Ogilvy et al. (1991) investigated the detectability of 2D low-conductivity. They showed that in the case of H-polarization, a higher apparent resistivity and smaller phase (lower than 45°) can be measured above the target. In the case of E-polarization, the cavity cannot be detected. This highlights the importance of using at least two transmitters, oriented nearly perpendicular to each other, if it is possible. Takács et al. (2005) compared the current density pseudosection with 2D VLF-EM anomalies. Pethő et al. (2006) investigated the response of near-surface targets for plane waves (VLF) and electric dipoles in TE and TM modes. Pethő (2012) and Vincze et al. (2024) present the application possibilities of the VLF method in Hungary.

By measuring the electrical component, it became possible to determine the apparent resistivity and, at the same time, to apply the 1D inversion previously developed in magnetotellurics. From the apparent resistivity and phase difference data measured at a VLF frequency, the parameters of a two-layer model can be calculated by assuming one of the three parameters to be known. The calculations are facilitated by the fact that the forward modeling of the 1D layered half-space can be solved with a simple recursive formula. In the case of a horizontally layered n-layer half-space, the parameters ρ_n (layer resistivities) and h_{n-1} (layer thickness) can be used to calculate the data ρ_a (apparent resistivity) and φ (phase) using a recursive formula (see Tutorial). The calculation should start with the impedance of the lowest layer:

$$Z_n = \sqrt{i\omega\mu_0\rho_n} \tag{14}$$

then the reflection coefficient occurring at the boundary of the next layer is calculated as

$$R_{n-1} = \frac{\sqrt{i\omega\mu_0\rho_{n-1}} - \sqrt{i\omega\mu_0\rho_n}}{\sqrt{i\omega\mu_0\rho_{n-1}} + \sqrt{i\omega\mu_0\rho_n}}$$
(15)

after that the impedance of the next layer can be calculated

$$Z_{n-1} = \sqrt{i\omega\mu_0\rho_{n-1}} \frac{1 - R_{n-1}\exp\left(-2\sqrt{\frac{i\omega\mu_0}{\rho_{n-1}}h_{n-1}}\right)}{1 + R_{n-1}\exp\left(-2\sqrt{\frac{i\omega\mu_0}{\rho_{n-1}}h_{n-1}}\right)}$$
(16)

The reflection coefficient and impedance of the next layer boundary can be calculated, until we reach the topmost, first layer, from whose impedance the apparent resistivity and phase values can be calculated

$$\rho_a = \frac{1}{u_{ro}} |Z_1|^2 \tag{17}$$

$$\rho_{a} = \frac{1}{\mu_{0}\omega} |Z_{1}|^{2}$$

$$\varphi = \tan^{-1} \frac{\text{Im}(Z_{1})}{\text{Re}(Z_{1})}$$
(17)

Numerous nomograms, recursion formulas and computer programs have been developed to estimate the model parameters. It should be noted that in the twolayer case, the phase deviation from 45° carries valuable information about the resistivity relationship of the lower and upper layers. If $\varphi < 45^{\circ}$, then $\rho_2 > \rho_1$, but for $\varphi > 45^{\circ}$, then $\rho_2 < \rho_1$.

The need to extend the narrow frequency range of the VLF band arose early on. Takács (1971) used a frequency range of 155 kHz and 629 kHz to solve various geological tasks (limestone, andesite, sandstone exploration). Pethő and Újszászi (1975) investigated the applicability of the radio-kip method for cave exploration. Stiefelhagen and Müller (1979) performed measurements in the 15-300 kHz range and confirmed their hydrogeological usefulness. Beamish (2000) compared the VLF and RMT methods in terms of layer resolution, see Figure 1.

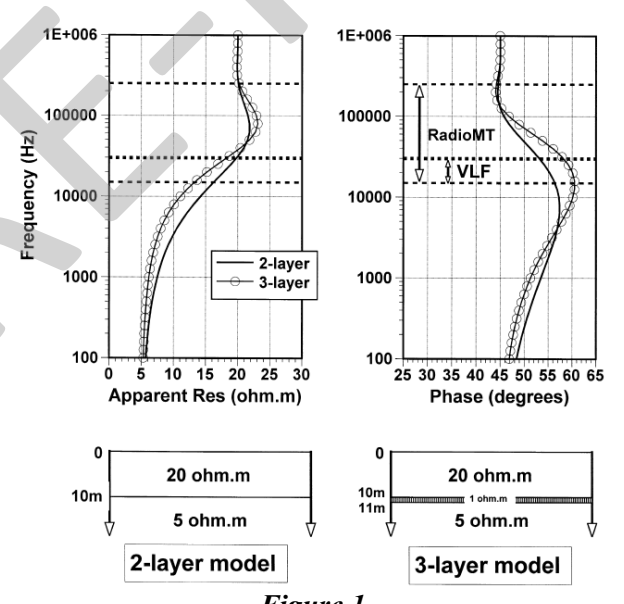
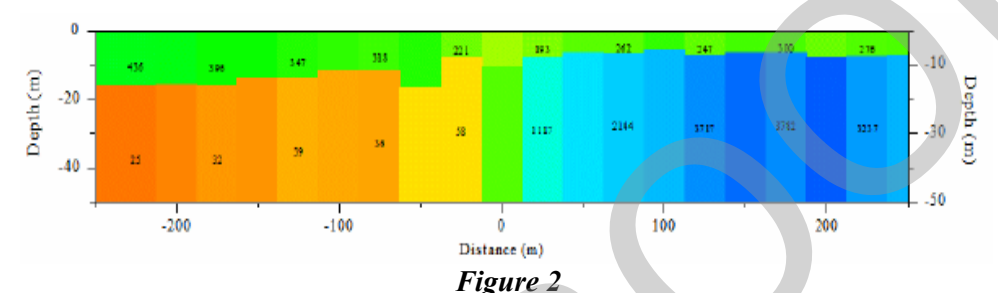


Figure 1

Evaluability analysis of two- and three-layer models in the case of VLF and RMT

The study demonstrates the importance of the extended frequency range of RMT in the investigation of 1D structures. In the case of two-dimensional effects, we find that in some cases even mono-frequency VLF measurements are able to approximate the structure.

Pirttijarvi (2006) developed a two-layer inversion with a known parameter-free lateral constraint for processing VLF-R measurements. This minimizes the model's roughness between neighboring points, resulting in a model with smooth variation (Occam inversion), see Figure 2.



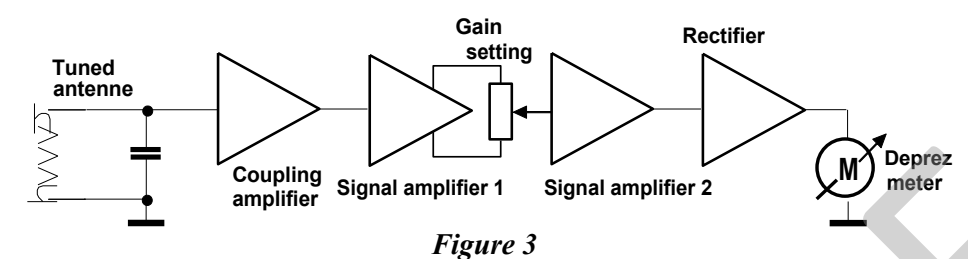
Laterally constrained two-layer inversion of VLF-R measurement data

Schmalz et al. (2007) published a similar inversion for radio-magneto-telluric data, where the number of layers could be increased. In addition, Rodi and Mackie (2001) also implemented a 2D inversion using the nonlinear conjugate gradient (NLCG) method.

Following in the footsteps of the previous ones, EMTOMO (2022) developed the VLF2DMF application, a program for 2D inversion of multifrequency VLF-EM data. 2D and 3D forward modeling is solved using finite element, finite difference, integral equation and scattering matrix formalism methods. For 2D and 3D inversion, linearized second-order Marquardt least squares (LSQ), nonlinear conjugate gradient (NLCG) or global optimization based very fast simulated annealing (VFSA) methods are commonly used.

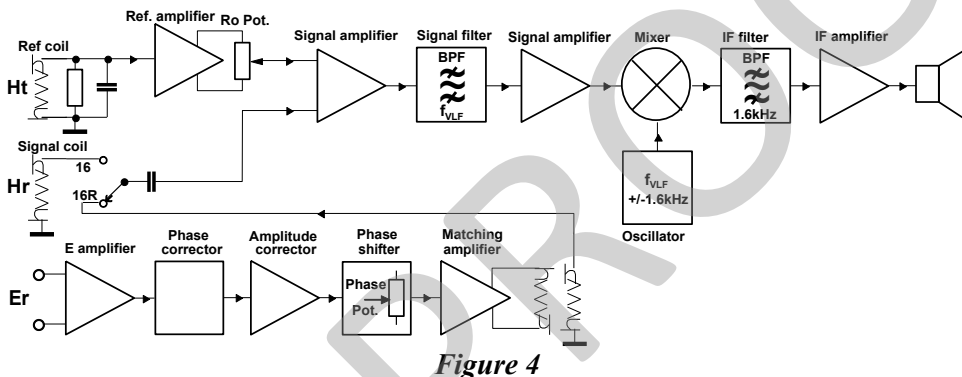
3. DEVELOPMENTS OF VLF INSTRUMENTS

It is valuable to review the development of VLF instruments because the structure of the initial RMT instruments was completely identical to that of VLF instruments, only with an extended frequency range. The simplest VLF receivers resemble a straight-line radio receiver, see Figure 3. The selection of the desired frequency is provided by a parallel LC circuit, which is the antenna of the instrument itself. VLF receivers with such a system are the Scintrex SE-81 and the Phoenix VLF-2 instrument.



Block diagram of a straight-forward VLF receiver

The first widely used VLF receiver, the Geonics EM16/16R instrument, uses the so-called heterodyne principle to increase selectivity, see Figure 4.



Schematic of Geonics EM16/16R

With the advent of digital CMOS circuits, various hybrid receivers were built, in which the selection of the reception frequency and the display of the measurement results are now done digitally, but the circuits ensuring selectivity still remain analog. Such VLF instruments include the Totem II instrument of Herz Instrument, the CNYN instruments of the University of Neuchatel, the Syscal VLF instrument of BRGM and the VDV-1 instrument of Geofyzika Brno. To ensure selectivity when using broadband antennas, hybrid filters and digital signal processing methods have begun to be used. Examples include the Iris Instrument T-VLF instrument, the ABEM Wadi instrument, the Scintrex Envi-VLF instrument, and the GEM System walking VLF sensor.

4. DEVELOPMENTS OF RMT INSTRUMENTS

In the early days, ordinary long-wave radio receivers were also used to receive signals from radio stations above the VLF band, e.g. by Takács (1971). The University of Neuchatel extended the frequency range of earlier VLF instruments to 240 kHz.

The first tensor RMT instrument was developed at Uppsala University in Sweden (Bastani, 2001) under the name EnviroMT. The five-channel recorder can

measure all three magnetic and both surface electric field components. It is the first RMT instrument that broke with the frequency-selective measurement technique, which can process only one transmitter signal at a time, and applied the Fourier transformation processing of time-domain recordings, which was already used in magnetotellurics. The frequency range 1-250 kHz was divided into two parts. In the frequency range 1-25 kHz, the broadband signal is recorded with 200 kHz sampling, while in the range 10-250 kHz, the broadband signal is recorded with 20 MHz sampling. The lower 1-25kHz range is used more with the CSMT transmitter, while the upper 10-250kHz range is used with VLF-LF radio transmitters. The electric field is measured with grounded dipoles 5-10 m apart, while the magnetic field components are measured with 30 cm long, 7.5 cm diameter coils.

The four-channel RMT-F1 instrument was developed at Saint Petersburg State University in collaboration with the University of Cologne and MicroKOR Tezkan and Saraev (2008). Originally, the instrument was designed to have four channels, which allowed the recording of two electrical and two magnetic channels with a 16-bit A/D converter in the frequency range of 10-1000 kHz. It recorded 16kSample (16x1024 sample/sec) packets with a sampling rate of 2.5 MHz. The improved version of the instrument, the RMT-F, also received a fifth channel for recording the vertical magnetic component, the frequency range was extended to 1 kHz and the recording was done in 64kSample (64x1024 sample/sec) packets.

The latest extended application development of the instrument is called ARMT-5. The instrument is suitable for measuring in audio and radio frequency ranges in the range of 0.1 Hz - 1 MHz. The recorder has two five 16-bit A/D converters for the 10-1000 kHz range with 400 and 4000 kHz sampling and 24-bit A/D converters for the 0.1-10000 Hz frequency range with 32 and 4 kHz sampling. A great advantage of the recorder is the continuous sampling up to 4 MHz and the online display of data in both the time and frequency domains.

Modern magnetotelluric instruments with antennas with an appropriate frequency range are also suitable for RMT measurements. The Metronix ADU-08E logger, for example, has a sampling rate of 256 Hz to 262 kHz, which in principle allows recording up to 131 kHz. The SHFT-02 sensor has a bandwidth of 1-300 kHz. The Geometrix Stratagem EH-5 instrument has a frequency range of 1 Hz to 96 kHz.

5. DESIGN CONSIDERATION FOR A MODERN RMT INSTRUMENT

To exploit the full range of possibilities offered by the method, it is worth preparing to measure all possible field components. Three mutually perpendicular induction broadband antennas and three measuring channels are required for a complete measurement of the magnetic field strength. Measurement of the electric field strength can be made on the surface of the ground or in the air. No current can flow perpendicular to the interface between the conductive half-space and the air, thus two pairs of mutually perpendicular electrodes on the surface are sufficient for the complete determination of the electric field. This can be a ground electrode to be inserted into the ground, or a capacitive electrode that allows continuous

measurements. In the conductive half-space, the vertical electric component is important for measurements in boreholes. In the air, however, the vertical electric component also appears when rising from the surface and the horizontal components also behave depending on the height. In the frequency range of the method, an electric dipole or rod antenna that is greatly shortened compared to the wavelengths can only be used to good effect. These have low sensitivity (effective height) and are very sensitive to proximity to humans or the ground. They are only suitable for aerial measurements.

The unambiguous determination of the position of the sensors can be solved by using three types of spatial sensors. The global position of the measurement point can be determined by GPS or now more commonly GNSS equipment, the deviation of the sensors from the horizontal can be determined by two perpendicular tilt-probe meters, and the angular position around the vertical axis can be determined by a magnetic compass. Recently, the precise determination of the global location coordinate was considered a very expensive and resourceintensive task. The location accuracy of simple, cheap and small solutions (car navigation), which was limited to approx. 5-10 m even under favorable reception conditions, in many cases did not satisfy the needs of high-resolution ground measurements. For sub-meter and sub-decimeter location accuracy, the use of larger and more expensive antennas and also additional cost-intensive RTK (realtime kinematic) was required. Nowadays, however, small GNSS modules have appeared and are rapidly spreading, capable of sub-meter accuracy in autonomous mode or sub-decimeter accuracy with RTK.

When reviewing the development of VLF and RMT instruments, we also saw that the most modern instruments have broadband magnetic antennas, high input impedance and low capacitance electrical input amplifiers and minimal additional analog circuits. The signals to be measured are digitized after a mandatory antialiasing low-pass filter, and then further signal processing is done digitally. Similar to the previously described analog principles ensuring frequency selectivity, mixing of the heterodyne system, bandpass filtering, and phase selective demodulation, all of these functions can also be performed in the digital space. If it is necessary to use an analog output device, for example a loudspeaker for acoustic indication, this can also be solved at the end of the signal processing, after digital-to-analog conversion, using minimal analog hardware elements (recombination filter, power amplifier). We have also shown earlier that the development of personal computers has long reached the level that real-time SDR (Software Defined Radio) in the RMT frequency range is not a problem. These capabilities have long been surpassed by laptops, notebooks, tablets and mobile phones. Many new geophysical instruments can be seen today equipped with field tablets. Moreover, these devices are equipped with almost unlimited data storage capacity and even the above-mentioned sensors (GNSS, compass, spirit level). In order to reduce consumption, weight and size, it makes sense to implement the aforementioned functions with target hardware. The new generation of 16/32-bit microcontrollers equipped with DSP (Digital Signal Processing) functions provides

excellent opportunities for solving the aforementioned tasks. The great advantage of DSP is that, for example, the large-bit multiplication operation required for fast Fourier transformation is not performed by machine routines with hundreds of instructions, but is performed in cycles of a few hours. To demonstrate that a real-time radio receiver operating in the RMT band is feasible, an Italian radio amateur Alberto di Bene (online) built a simple radio receiver operating in the 8-900 kHz range using the Discovery development board built with the STM32F429 microcontroller and some additional analog circuitry, see Figure 5.

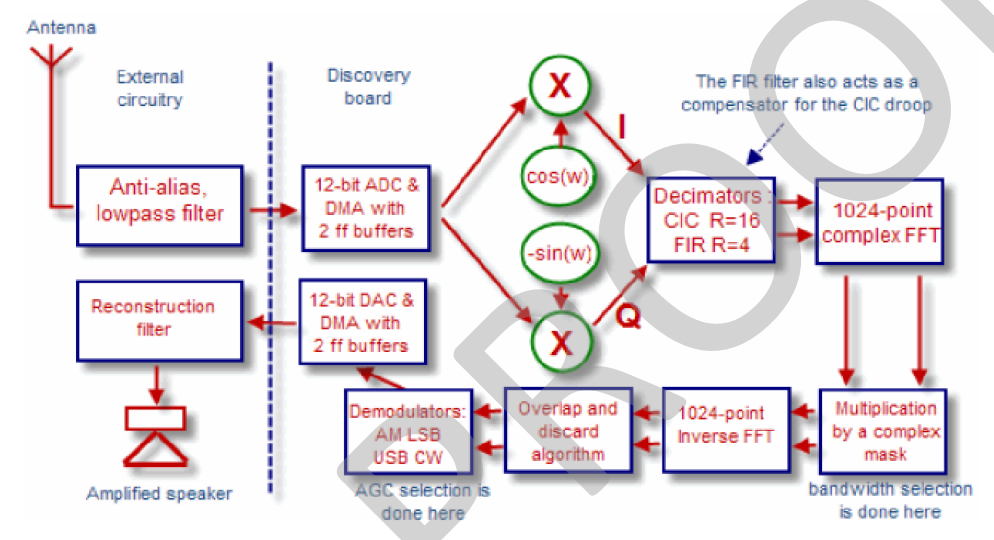


Figure 5
Direct receiver for a frequency of 8-900 kHz

6. RADIO TRANSMITTERS IN THE VLF AND RMT BAND RECEIVABLE IN HUNGARY

The frequency range from 10 kHz to 1 MHz includes the VLF (very low frequency) band, which is used for submarine communications and includes time signal transmitters, as well as the LF (low frequency) and partly the MF (medium frequency) bands, which include broadcast transmitters and amateur bands.

Until the 70s and 80s, several transmitters operated continuously in the VLF band, in the 15.1-24.0 kHz range, which then ceased to operate one after another. Instead, a smaller number of new transmitters were launched in the 18.1-26.7 kHz range. There is also a stably operating transmitter station in the 40-100 kHz range. The best known of them is the DCF77 time signal transmitter (77.5 kHz).

There are also stable transmitters in the 100-153 kHz range, the source of which has yet to be investigated. The previously bustling life in the LF and MF bands has now died down, but a few usable transmitters remain.

It is clear from Table 2 that the distribution of frequencies that can be received in good quality in Hungary is not uniform. The frequencies that are close to each

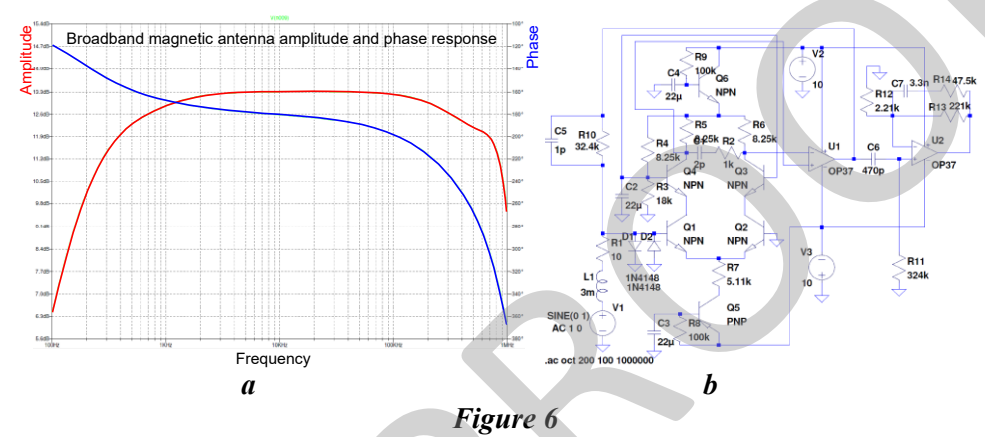
other, arriving from different directions, provide an opportunity to calculate the invariant apparent resistivity.

Table 2 Radio transmitters in the RMT band receivable in Hungary (based on own measurements)

18.1 kHz Russia Krasnodar RDL 18.3 kHz France Rosnay HWU 19.6 kHz 30 kW UK Anthorn CQD 20.27 kHz Italy Tavolara ICV 21.75 kHz France Rosnay HWU 22.1 kHz UK Anthorn CQD 23.4 kHz 800 kW Germany Rhauderfehn DHO38 24.0 kHz 1000 kW USA Cutler, Maine NAA 26.7 kHz Turkey Bafa TBB 40.4 kHz Sweden SAS3 45.9 kHz Sweden SAS3 45.9 kHz UK Niscemi NSY 51.95 kHz UK Niscemi NSY 51.95 kHz UK Anthorn MSF 62.6 kHz 17 kW UK Anthorn MSF 65.8 kHz France Kerlouan FUE 66.6 kHz 10 kW Russia Moscow RBU 77.5 kHz <th>Frequency</th> <th>Power</th> <th>Country</th> <th>Region</th> <th>Call Sign</th>	Frequency	Power	Country	Region	Call Sign
19.6 kHz	18.1 kHz		Russia	Krasnodar	RDL
Tavolara CV Prance Rosnay HWU Rosnay HWU Rosnay Rosnay HWU Rosnay Ros	18.3 kHz		France	Rosnay	HWU
21.75 kHz France Rosnay HWU 22.1 kHz UK Anthorn CQD 23.4 kHz 800 kW Germany Rhauderfehn DHO38 24.0 kHz 1000 kW USA Cutler, Maine NAA 26.7 kHz Turkey Bafa TBB 40.4 kHz Sweden Grimeton SRC 44.2 kHz Sweden SAS3 45.9 kHz 250 kW Italy Niscemi NSY 51.95 kHz UK Anthorn MSF 62.6 kHz France La Regime FUG 65.8 kHz France Kerlouan FUE 66.6 kHz 10 kW Russia Moscow RBU 77.5 kHz 50 kW Germany Mainflingen DCF77 81 kHz UK GYN2 81.8 kHz T12.0 kHz SSR Antena Sat. 128.9 kHz 133.7 kHz SSR Antena Sat. 153 kHz 200 kW Romania Brasov SSR Antena Sat.	19.6 kHz	30 kW	UK	Anthorn	CQD
22.1 kHz UK Anthorn CQD 23.4 kHz 800 kW Germany Rhauderfehn DHO38 24.0 kHz 1000 kW USA Cutler, Maine NAA 26.7 kHz Turkey Bafa TBB 40.4 kHz Sweden Grimeton SRC 44.2 kHz Sweden SAS3 45.9 kHz 250 kW Italy Niscemi NSY 51.95 kHz UK MSF SAS3 45.9 kHz 17 kW UK Anthorn MSF 60.0 kHz 17 kW UK Anthorn MSF 62.6 kHz France Kerlouan FUE 66.6 kHz 10 kW Russia Moscow RBU 77.5 kHz 50 kW Germany Mainflingen DCF77 81 kHz UK GYN2 81.8 kHz Sep.6 kHz Sep.6 kHz Sep.6 kHz 113.7 kHz Sep.6 kHz Sep.6 kHz Sep.6 kHz 135.4 kHz Sep.6 kHz <td< td=""><td>20.27 kHz</td><td></td><td>Italy</td><td>Tavolara</td><td>ICV</td></td<>	20.27 kHz		Italy	Tavolara	ICV
23.4 kHz 800 kW Germany Rhauderfehn DHO38 24.0 kHz 1000 kW USA Cutler, Maine NAA 26.7 kHz Turkey Bafa TBB 40.4 kHz Sweden Grimeton SRC 44.2 kHz Sweden SAS3 45.9 kHz 250 kW Italy Niscemi NSY 51.95 kHz UK Anthorn MSF 60.0 kHz 17 kW UK Anthorn MSF 62.6 kHz France La Regime FUG 65.8 kHz France Kerlouan FUE 66.6 kHz 10 kW Russia Moscow RBU 77.5 kHz 50 kW Germany Mainflingen DCF77 81 kHz UK GYN2 81.8 kHz 112.0 kHz 113.7 kHz 113.7 kHz 113.7 kHz 135.4 kHz SSR Antena Sat. 153 kHz 200 kW Romania Brasov SSR Antena Sat. 160 kW Morocco	21.75 kHz		France	Rosnay	HWU
24.0 kHz 1000 kW USA Cutler, Maine NAA 26.7 kHz Turkey Bafa TBB 40.4 kHz Sweden Grimeton SRC 44.2 kHz Sweden SAS3 45.9 kHz 250 kW Italy Niscemi NSY 51.95 kHz UK NSY UK MSF 60.0 kHz 17 kW UK Anthorn MSF 62.6 kHz France La Regime FUG 65.8 kHz France Kerlouan FUE 66.6 kHz 10 kW Russia Moscow RBU 77.5 kHz 50 kW Germany Mainflingen DCF77 81 kHz UK GYN2 81.8 kHz S9.6 kHz 112.0 kHz 113.7 kHz 113.7 kHz 135.4 kHz SSR Antena Sat. 153 kHz 200 kW Romania Brasov SSR Antena Sat. 162 kHz 800 kW France Allouis TDF, ALS162 171 kHz 1600 kW </td <td>22.1 kHz</td> <td></td> <td>UK</td> <td>Anthorn</td> <td>CQD</td>	22.1 kHz		UK	Anthorn	CQD
26.7 kHz Turkey Bafa TBB 40.4 kHz Sweden Grimeton SRC 44.2 kHz Sweden SAS3 45.9 kHz 250 kW Italy Niscemi NSY 51.95 kHz UK MSF 60.0 kHz 17 kW UK Anthorn MSF 62.6 kHz France La Regime FUG 65.8 kHz France Kerlouan FUE 66.6 kHz 10 kW Russia Moscow RBU 77.5 kHz 50 kW Germany Mainflingen DCF77 81 kHz UK GYN2 81.8 kHz Sep. 6 kHz I12.0 kHz 113.7 kHz I13.7 kHz I13.7 kHz 135.4 kHz Sep. 6 kHz Sep. 6 kHz 171 kHz 1600 kW Romania Brasov SSR Antena Sat. 162 kHz 800 kW France Allouis TDF, ALS162 171 kHz 1600 kW Morocco Nador	23.4 kHz	800 kW	Germany	Rhauderfehn	DHO38
40.4 kHz Sweden Grimeton SRC 44.2 kHz Sweden SAS3 45.9 kHz 250 kW Italy Niscemi NSY 51.95 kHz UK NSY UK NSY 60.0 kHz 17 kW UK Anthorn MSF 62.6 kHz France La Regime FUG 65.8 kHz France Kerlouan FUE 66.6 kHz 10 kW Russia Moscow RBU 77.5 kHz 50 kW Germany Mainflingen DCF77 81 kHz UK GYN2 81.8 kHz Sector GYN2 81.8 kHz Sector Sector 89.6 kHz Sector Sector 113.7 kHz Sector Sector 133.7 kHz Sector Sector 153 kHz 200 kW Romania Brasov Sector 162 kHz 800 kW France Allouis TDF, ALS162 171 kHz 1600 kW Morocco	24.0 kHz	1000 kW	USA	Cutler, Maine	NAA
44.2 kHz Sweden SAS3 45.9 kHz 250 kW Italy Niscemi NSY 51.95 kHz UK UK NSY 60.0 kHz 17 kW UK Anthorn MSF 62.6 kHz France La Regime FUG 65.8 kHz France Kerlouan FUE 66.6 kHz 10 kW Russia Moscow RBU 77.5 kHz 50 kW Germany Mainflingen DCF77 81 kHz UK GYN2 81.8 kHz S9.6 kHz T12.0 kHz 113.7 kHz T12.0 kHz T13.7 kHz 135.4 kHz SSR Antena Sat. TDF, ALS162 171 kHz 1600 kW Morocco Nador	26.7 kHz		Turkey	Bafa	TBB
45.9 kHz 250 kW Italy Niscemi NSY 51.95 kHz UK UK MSF 60.0 kHz 17 kW UK Anthorn MSF 62.6 kHz France La Regime FUG 65.8 kHz France Kerlouan FUE 66.6 kHz 10 kW Russia Moscow RBU 77.5 kHz 50 kW Germany Mainflingen DCF77 81 kHz UK GYN2 81.8 kHz S9.6 kHz I12.0 kHz 113.7 kHz I13.7 kHz I13.7 kHz 135.4 kHz I135.4 kHz SSR Antena Sat. 153 kHz 200 kW Romania Brasov SSR Antena Sat. 162 kHz 800 kW France Allouis TDF, ALS162 171 kHz 1600 kW Morocco Nador	40.4 kHz		Sweden	Grimeton	SRC
51.95 kHz UK Anthorn MSF 62.6 kHz France La Regime FUG 65.8 kHz France Kerlouan FUE 66.6 kHz 10 kW Russia Moscow RBU 77.5 kHz 50 kW Germany Mainflingen DCF77 81 kHz UK GYN2 81.8 kHz 89.6 kHz 112.0 kHz 113.7 kHz 128.9 kHz 133.7 kHz 135.4 kHz Romania Brasov SSR Antena Sat. 162 kHz 800 kW France Allouis TDF, ALS162 171 kHz 1600 kW Morocco Nador	44.2 kHz		Sweden		SAS3
60.0 kHz 17 kW UK Anthorn MSF 62.6 kHz France La Regime FUG 65.8 kHz France Kerlouan FUE 66.6 kHz 10 kW Russia Moscow RBU 77.5 kHz 50 kW Germany Mainflingen DCF77 81 kHz UK GYN2 81.8 kHz 112.0 kHz 113.7 kHz 113.7 kHz 128.9 kHz 133.7 kHz 135.4 kHz Romania Brasov SSR Antena Sat. 153 kHz 200 kW France Allouis TDF, ALS162 171 kHz 1600 kW Morocco Nador Radio Méditeranée	45.9 kHz	250 kW	Italy	Niscemi	NSY
62.6 kHz France La Regime FUG 65.8 kHz France Kerlouan FUE 66.6 kHz 10 kW Russia Moscow RBU 77.5 kHz 50 kW Germany Mainflingen DCF77 81 kHz UK GYN2 81.8 kHz 112.0 kHz 113.7 kHz 113.7 kHz 128.9 kHz 133.7 kHz 135.4 kHz Romania Brasov SSR Antena Sat. 162 kHz 800 kW France Allouis TDF, ALS162 Radio Méditeranée Radio Méditeranée	51.95 kHz		UK		
65.8 kHz France Kerlouan FUE 66.6 kHz 10 kW Russia Moscow RBU 77.5 kHz 50 kW Germany Mainflingen DCF77 81 kHz UK GYN2 81.8 kHz 89.6 kHz 112.0 kHz 113.7 kHz 128.9 kHz 133.7 kHz 135.4 kHz Romania Brasov SSR Antena Sat. 162 kHz 800 kW France Allouis TDF, ALS162 171 kHz 1600 kW Morocco Nador Radio Méditeranée	60.0 kHz	17 kW	UK	Anthorn	MSF
66.6 kHz 10 kW Russia Moscow RBU 77.5 kHz 50 kW Germany Mainflingen DCF77 81 kHz UK GYN2 81.8 kHz UK GYN2 112.0 kHz 112.0 kHz 113.7 kHz 128.9 kHz 133.7 kHz 135.4 kHz 153 kHz 200 kW Romania Brasov SSR Antena Sat. 162 kHz 800 kW France Allouis TDF, ALS162 171 kHz 1600 kW Morocco Nador Radio Méditeranée	62.6 kHz		France	La Regime	FUG
77.5 kHz 50 kW Germany Mainflingen DCF77 81 kHz UK GYN2 81.8 kHz S9.6 kHz S9.6 kHz 112.0 kHz S13.7 kHz S13.7 kHz 128.9 kHz S133.7 kHz S135.4 kHz 153 kHz 200 kW Romania Brasov SSR Antena Sat. 162 kHz 800 kW France Allouis TDF, ALS162 171 kHz 1600 kW Morocco Nador	65.8 kHz		France	Kerlouan	FUE
81 kHz UK GYN2 81.8 kHz 89.6 kHz 112.0 kHz 113.7 kHz 128.9 kHz 133.7 kHz 133.7 kHz 135.4 kHz SSR Antena Sat. 153 kHz 200 kW Romania Brasov SSR Antena Sat. 162 kHz 800 kW France Allouis TDF, ALS162 171 kHz 1600 kW Morocco Nador	66.6 kHz	10 kW	Russia	Moscow	RBU
81.8 kHz 89.6 kHz 112.0 kHz 113.7 kHz 128.9 kHz 133.7 kHz 135.4 kHz 153 kHz 200 kW Romania Brasov SSR Antena Sat. 162 kHz 800 kW France Allouis TDF, ALS162 Radio Méditeranée	77.5 kHz	50 kW	Germany	Mainflingen	DCF77
89.6 kHz 112.0 kHz 113.7 kHz 128.9 kHz 133.7 kHz 135.4 kHz 153 kHz 200 kW Romania Brasov SSR Antena Sat. 162 kHz 800 kW France Allouis TDF, ALS162 Radio Méditeranée	81 kHz		UK		GYN2
112.0 kHz 113.7 kHz 128.9 kHz 133.7 kHz 135.4 kHz 153 kHz 200 kW Romania Brasov SSR Antena Sat. 162 kHz 800 kW France Allouis TDF, ALS162 Radio Méditeranée	81.8 kHz				
113.7 kHz 128.9 kHz 133.7 kHz 135.4 kHz 153 kHz 200 kW Romania Brasov SSR Antena Sat. 162 kHz 800 kW France Allouis TDF, ALS162 171 kHz 1600 kW Morocco Nador Radio Méditeranée	89.6 kHz				
128.9 kHz 133.7 kHz 135.4 kHz 135.4 kHz 153 kHz 200 kW Romania Brasov SSR Antena Sat. 162 kHz 800 kW France Allouis TDF, ALS162 171 kHz 1600 kW Morocco Nador Radio Méditeranée	112.0 kHz				
133.7 kHz 135.4 kHz 135.4 kHz Romania 153 kHz 200 kW Romania Brasov SSR Antena Sat. SSR Antena Sat. 162 kHz 800 kW France Allouis TDF, ALS162 Radio Méditeranée	113.7 kHz				
135.4 kHz 153 kHz 200 kW Romania Brasov SSR Antena Sat. 162 kHz 800 kW France Allouis TDF, ALS162 Radio Méditeranée	128.9 kHz				
153 kHz 200 kW Romania Brasov SSR Antena Sat. 162 kHz 800 kW France Allouis TDF, ALS162 171 kHz 1600 kW Morocco Nador					
162 kHz 800 kW France Allouis TDF, ALS162 171 kHz 1600 kW Morocco Nador Radio Méditeranée	135.4 kHz				
171 kHz 1600 kW Morocco Nador Radio Méditeranée	153 kHz	200 kW	Romania	Brasov	SSR Antena Sat.
II/I kHz 1600 kW Morocco Nador I	162 kHz	800 kW	France	Allouis	
Internat.	171 kHz	1600 kW	Morocco	Nador	
189 kHz 300 kW Iceland Hellissandur RÚV 1/2	189 kHz	300 kW	Iceland	Hellissandur	
198 kHz 500 kW UK Droitwich BBC Radio 4 AM					
225 kHz 1000 kW Poland Solec Kujawski Polskie Radio					
252 kHz 1500/750 kW Algeria Tipaza Radio Algérie					

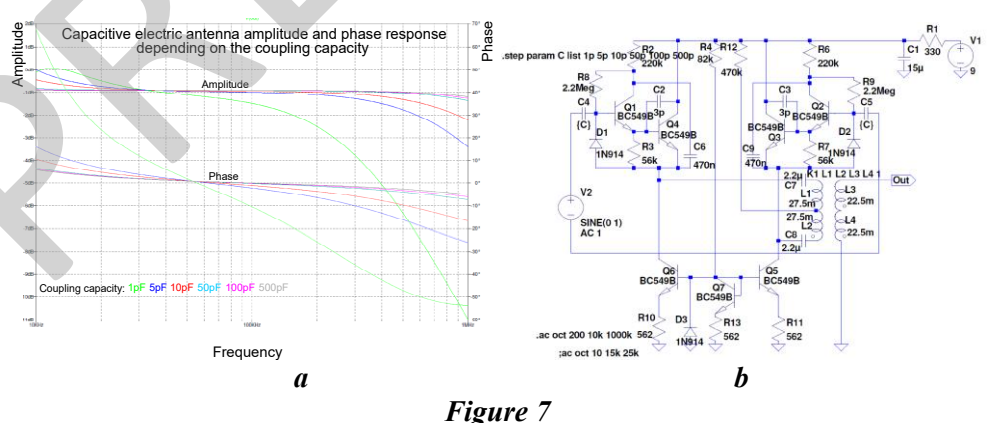
7. DESIGN CONSIDERATION FOR RMT INSTRUMENT SENSOR

To detect the magnetic components of the electromagnetic field, it is advisable to use a broadband antenna whose amplitude and phase shift are uniform or at least do not vary sharply in the required frequency range. Such a magnetic antenna can be produced using the principle of flux feedback. Figure 6a shows the amplitude and phase progression of an implementation. Figure 6b shows the circuit diagram of the implementation.



Frequency and phase response (a) and circuit diagram (b) of H-sensor.

A capacitive antenna with a suitable linear transfer can be realized with a preamplifier with a high input resistance and a small capacitance, which also has a low quiescent input current. In the figure below, we examine the transfer of the capacitive antenna with coupling capacitances of 1pF, 5pF, 10pF, 50pF, 100pF and 500pF. It is clear that the linear transition can be ensured with coupling above 5pF. Figure 7a shows the amplitude and phase progression of an implementation. Figure 7b shows the circuit diagram of the implementation.



Frequency and phase response (a) and circuit diagram (b) of the E-sensor.

8. CONCLUSIONS

In a modern RMT instrument, it is advisable to measure as many parameters as possible, which are generally three magnetic and three electrical components. On land and water, only two electrical components can be conveniently measured. In the air, it is theoretically possible to measure all three electrical components, but in practice, it is more feasible to measure the three magnetic components. For measurements on the ground, the condition for moving measurements is the use of a capacitive electric dipole. With high input resistance and large capacitance preamplifiers, uniform transmission can be achieved if the coupling of the capacitive sensors to the ground is not worse than 5 pF. It is advisable to design the magnetic antennas to be broadband and provide them with a preamplifier based on the principle of flux feedback. Determining the position of the sensors is of fundamental importance. With modern GNSS modules, positioning accuracy of around 1 m can be achieved even in autonomous cases. The inclination of the sensors should be measured with two-way inclinometer sensors. The azimuth of the sensors can be determined with a semiconductor magnetic compass. It also provides a suitable solution for tensor measurements, recording short, broadband signal packets during measurements, and then digitally measuring the selected frequencies using SDR and DSP. An important goal is to create a profile or map image from the measurement results in real time. The use of 1D-LCI seems suitable for this purpose.

ACKNOWLEDGMENTS

I am grateful to Professor Ernő Takács for introducing me to the exciting world of electromagnetic methods. I am grateful to the former ELGI for the opportunity to become familiar with the practical application of numerous electromagnetic instruments and methods. Finally, I would like to thank my supervisors, Professors Mihály Dobróka and Gábor Pethő, for their support in this topic.

REFERENCES

- Bastani, M. (2001). EnvitoMT: A new controlled source/radio magnetotelluric system, PhD dissertation, University Uppsala, 2001.
- Beamish, D. (2000). Quantitative 2D VLF data interpretation. Journal of Applied Geophysics, 45, pp. 33-47.
- Bezdova, V., Segeth, K.(1982). On the resolving power of the VLF method, Pure and Applied Geophysics, 120(2), pp. 348-364.
- Cagniard, L. (1953). Basic theory of the magneto-telluric method of geophysical prospecting. Geophysics, 18(3), pp.603-635.
- di Bene, A. ARM Radio: a project for the ARM MCU Design Contest. Available online: https://www.i2phd.org/code/ARM-Radio.pdf, (accessed on 1 December 2024).

- Dosso, H. W. (1962). The magnetic field at the surface of a stratified flat conductor in field of planewaves with application to geophysics. Canadian Journal of Physics, 40(11), pp.1583-1592.
- Dosso, H. W. (1965a). The electric and magnetic fields in a stratified flat conductor for incident planewaves. Canadian Journal of Physics, 43(5), pp.898-909.
- Dosso, H. W. (1965b). A multilayer conducting earth in the field of planewaves. Canadian Journal of Physics, 44(1), pp.81-89.
- EMTOMO, (2022). VLF2DMF A program for 2-D inversion of multifrequency VLF-EM data. Operational Manual.
- Farkas, I.(1978). VLF invariáns ellenállás módszer. A Magyar Állami Eötvös Loránd Geofizikai Intéztet 1978. évi jelentése, pp. 79-80.
- Fraser, D. C. (1969). Contouring of VLF-EM data. Geophysics, 34(6), pp.958-967.
- Kaikkonen, P. (1979). Numerical VLF modeling, Geophysical Prospecting, 27(4), pp. 815-834
- Karous, M., Hjelt, S. E. (1983). Linear filtering of VLF dip-angle measurements. Geophysical Prospecting, 31, pp. 782-794.
- McNeil, J.D., Labson, V. F. (1991). Geological mapping using VLF radio fields. Electromagnetic Methods in Applied Geophysics, Chp.7., pp.521-640.
- Ogilvy, R. D., Cuadra, A., Jackson, P. D., Monte, J. L. (1991). Detection of an air-filled drainage gallery by the VLF resistivity method, Geophysical Prospecting, 39, pp. 845-859.
- Olsson, O. (1983). Computation of VLF response over half-plane and wedge models, Geophysical Prospectings, 31, pp. 171-191.
- Paterson, N. R. and Ronka, V. (1970). Five years of surveying with the very low frequency electromagnetic method. Geoexploration, 9, pp.7-26.
- Pedersen, L. B. (1998). Tensor VLF measurements: Our first experiences. Exploration Geophysics, 29, pp. 52-57.
- Pethő, G. (2012). Geological application of the VLF method, Geosciences and Engineering, 1(2), pp. 129-139.
- Pethő, G., Ficsór, L., Szabó, I. (2006). Comparison of 2-D VLF and 2.5D HED's far field regime EM field, microCAD Conference Paper, 2006, Miskolc, pp. 35-40
- Pethő, G., Újszászi, J. (1975). Barlang kutatás radiokip módszerrel. Magyar Geofizika, 16(5), pp. 181-186.
- Pirttijarvi, M. (2006). 2LAYINV Laterally constrained two-layer inversion of VLF-R measurements. Operating Manual.

- Rodi, W., Mackie, RL. (2001). Nonlinear conjugate gradient algorithm for 2-D magnetotelluric inversion, Geophysics, 66(1), pp. 174-187.
- Saydam, A. S. (1981). Verylow-frequency electromagnetic interpretation using tilt angle and ellipticity measurement. Geophysics, 46(11), pp. 1594-1605.
- Schmalz, T. et al. (2007). 1D-laterally constraint inversion (1D-LCI) of radiomagnetotelluric data, 22. Kolloquium Electromagnetische Tiefenforshung.
- Stiefelhagen, W, Müller, I. (1979). Radiofrequency electromagnetics (RFEM): VLF-EM extended to hydrogeological problems. 59th Meeting of EAGE, Geneva, 1979.
- Takács, E. (1971). Tapasztalatok a rádiokipmódszer alkalmazásában. Magyar Geofizika, 12(4), pp.148-160.
- Takács, E., Pethő, G., Szabó, I. (2005). Comparativ investigation about the applicability of current density pseudo sections in the interpretation of 2D VLF vertical magnetic anomalies, Acta Geod. Geoph. Hung., 40(4), pp. 127-146.
- Teemull, F. A., Crossley, D. J. (1982). Inversion of VLF data for simple lateral inhomogeneities, Geophysical Application of surface wave impedance measurements, Geological Survey of Canada, pp. 79-86.
- Tezkan, B., Saraev, A. (2008). A new broadband radiomagnetotelluric instrument application to near surface investigation, Near Surface Geophysics, 6(4), pp. 245-252.
- Tutorial 1D Forward Modelling (Magnetotelluric). Available online: https://www.digitalearthlab.com/tutorial/tutorial-1d-mt-forward/ (accessed on 1 December 2024).
- Vincze, L., Németh, N., Pethő, G. (2024). Eredmények és tapasztalatok a VLF módszer területén, Magyar Geofizika, 65(1), pp. 27-45.
- Wait, J. R. (1953). Propagation of radio waves over a stratified ground. Geophysics, 18(2), pp.416-422.